

# Polarization Position Angle Swings caused by Relativistic Effects

Shan-Jie Qian and Xi-Zhen Zhang

National Astronomical Observatories, Chinese Academy of Sciences, Beijing 100012;  
rqsj@bao.ac.cn

Received 2002 September 12; accepted 2002 December 2

**Abstract** Polarization position angle swings of  $\sim 180^\circ$  observed in extragalactic radio sources are a regular behavior of variability in polarization. They should be due to some kind of physically regular process. We consider relativistic shocks which propagate through and ‘illuminate’ regular configurations of magnetic field, producing polarization angle swing events. Two magnetic field configurations (force-free field and homogeneous helical field) are considered to demonstrate the results. It is shown that the properties of polarization angle swings and the relationship between the swings and variations in total and polarized flux density are critically dependent on the configuration of magnetic field and the dynamical behavior of the shock. In particular, we find that in some cases polarization angle swings can occur when the total and polarized flux densities only vary by a very small amount. These results may be useful for understanding the polarization variability with both long and short timescales observed in extragalactic radio sources.

**Key words:** radio continuum: galaxies — polarization — galaxies: magnetic fields

## 1 INTRODUCTION

In the study of compact extragalactic radio sources, linear polarization variability has been observed for more than 20 years, especially for violently variable radio sources (blazars). The timescale of the variability ranges from weeks (even days) to years, usually appearing during radio outbursts (Aller 1999). Radio outbursts are enhanced synchrotron radiation emitted by disturbances propagating down the magnetized jets. Relativistic shocks (transverse and oblique) have been suggested to explain these polarization variations (Hughes et al. 1989; Aller et al. 2002). For the long timescale polarization variability, comparisons of theoretical models with multifrequency observations and VLBI mapping of radio outbursts have shown that shock models are plausible for explaining the observed properties of the outbursts, including their intensity and polarization.

Very short timescales of polarization variability, which are also observed in extragalactic radio sources, range from  $\sim 1$  day to less than an hour (so called intraday polarization variability;

Wagner & Witzel 1995). For intraday polarization variability, both intrinsic mechanisms (Qian et al. 1991, 2002; Marscher et al. 1992; Marscher 1996; Quirreback et al. 1989; Gopal-Krishna & Wiita 1992) and extrinsic mechanisms (mainly refractive scintillation, Rickett et al. 1995, 2002; Qian et al. 2001; Simonetti 1991) have been proposed.

VLBI polarization observations have been carried out by Gabuzda & Cawthorne (2000) to study polarization variability in intraday variability (IDV, hereafter) sources. It is found that in several cases significant polarization variations were not accompanied by substantial total flux variations. This kind of polarization variations cannot be explained in terms of refractive scintillation, because in the scintillation scenario, polarization variations are caused through the flux variations in the polarized components. Gabuzda & Cawthorne (2000) argued that there is mounting evidence that a substantial fraction of IDV includes an appreciable or even dominant, intrinsic component.

Generally, for both long- and short-timescale polarization variability, the relationship between the variation in polarization and in intensity is complicated (Aller 1999; Qian et al. 2002), and the characteristics of this relationship may be useful to disclose the origin of the polarization variations.

Polarization position angle swings are a particularly interesting phenomenon for the study of polarization variability in extragalactic radio sources, because these regular variability may provide significant information about the physical processes in the source and distinguish between different models.

Large swings of polarization angle have been observed during radio outbursts (e.g. Ledden & Aller 1978) and usually interpreted in terms of relativistic aberration effects which are caused by relativistic shocks propagating along the jet and illuminating a regular magnetic field or through the dynamic behavior of the shock (acceleration or motion along curved trajectories): e.g., Blandford & Königl (1979); Björnson (1982); Königl & Choudhuri (1985b); Qian (1992). Two-component models were also proposed to explain polarization angle swings, in which the latter are produced by the vector combination of the polarization from a variable component (shock) and a steady polarized component, with their polarization angles differing approximately by  $90^\circ$  (Qian 1993).

Polarization angle swings of  $\sim 180^\circ$  have also been observed in intraday variable sources (for example, in the QSO 0917+624 (Quirreback et al. 1989), and in the QSO 1150+812 (Kochenov & Gabuzda 1999). Refractive scintillation models proposed until now could not explain this kind of continuous polarization angle swings (Rickett et al. 1995; Simonetti 1991). Improved scintillation models are required in order to explain these rapid polarization angle swings. In contrast, as for the long timescale polarization angle swings, these intraday polarization angle swings could be explained in terms of relativistic shock models (Qian et al. 1991, 2002).

As pointed out by Björnson (1982), in the study of the origin of polarization angle swings, it is important to study the relationship between the swing and the variability in polarized and total flux density in order to distinguish between different models. For example, some models predict that the polarized flux density is at its minimum when the rate of swing is greatest, but other models predict that polarized flux density remains almost constant during the swing.

In this paper we will consider a mechanism of large polarization angle swings, in which relativistic shocks propagate through different regular magnetic field configurations, so showing different relationships between the polarization angle swing and the variability in polarized and total flux density.

## 2 MODELS FOR POLARIZATION ANGLE SWING

We will consider two cases: (1) a relativistic shock propagates through regular magnetic field configurations and produces a polarization angle swing by illuminating rotating magnetic fields; (2) polarization angle swings are caused by relativistic aberration effects through the change of the viewing angle (or aberration angle) due to the dynamical behavior of the shock.

### 2.1 Geometry and Magnetic Field Configuration

Before doing so, we first describe the magnetic field configurations which will be used in this paper. The geometry for describing the magnetic field and the relativistic jet flow is sketched in Figure 1. The jet flow is assumed to move along x-axis with velocity  $c\beta$ . Let  $\vec{n}$  be the unit vector directed to the observer, which is located in the plane  $(x, z)$  at a viewing angle  $\theta$ . The aberration angle will be designated as  $\theta_*$ .

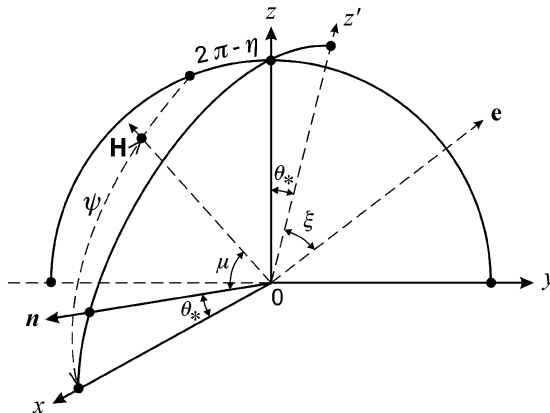


Fig. 1 Geometry of the magnetic field configuration.

When we study polarization angle swings in extragalactic radio sources caused by relativistic shocks propagating along the jet, we need to consider different kinds of magnetic field configuration because the properties of polarization angle swing are strongly dependent on the latter. We consider two field configurations: homogeneous helical field and force-free field.

#### 2.1.1 Homogeneous Helical Field

We first consider a simple case: a homogeneous helical field. As we will see that, in this case, some characteristics of the polarization angle swing and polarized flux variability may be particularly interesting and useful for understanding the observed polarization variability in extragalactic radio sources. The magnetic field can be simply described as

$$H_x = H \cos\psi, \quad (1)$$

$$H_y = H \sin\psi \cos\eta, \quad (2)$$

$$H_z = H \sin\psi \sin\eta, \quad (3)$$

where the magnetic field strength  $H$  is constant,  $\psi$  is the pitch angle,  $\eta = 2\pi x/\lambda$  is the azimuthal angle, and  $\lambda$  is the wavelength on which the field rotates by  $2\pi$ .

### 2.1.2 Force-free field

Königl & Choudhuri (1985a) have studied minimum-energy field configurations in magnetic-pressure dominated jets with dissipation by considering the conservation of magnetic helicity which determines the properties of twists and turbulence. They found that the structure of the magnetic field is a non-axisymmetric force-free field consisting of mode  $m=0$  and mode  $m=1$  (see Königl & Choudhuri 1985a). Mode  $m=1$  consists of two oppositely directed flux tubes that are wrapped around each other. We assume that for compact relativistic jets this kind of field configuration is also applicable. Since in the general case mode  $m=1$  dominates over mode  $m=0$ , we will apply mode  $m=1$  to describe the force-free field configuration of the jet. Substituting the appropriate numerical values into the formulae given by Königl & Choudhuri (1985a) we obtain the following expressions in cylindrical coordinates  $(x, r, \phi)$ :

$$H_x = H_0 J_1(r_\lambda) \cos(\phi + 2\pi x/\lambda), \quad (4)$$

$$H_y = H_r \cos \phi - H_\phi \sin \phi, \quad (5)$$

$$H_z = H_r \sin \phi + H_\phi \cos \phi. \quad (6)$$

Here

$$H_r = -0.4386 H_0 \left[ J_0(r_\lambda) + 1.49 \frac{J_1(r_\lambda)}{r_\lambda} \right] \sin\left(\phi + \frac{2\pi x}{\lambda}\right), \quad (7)$$

$$H_\phi = -1.092 H_0 \left[ J_0(r_\lambda) - 0.5981 \frac{J_1(r_\lambda)}{r_\lambda} \right] \cos\left(\phi + \frac{2\pi x}{\lambda}\right), \quad (8)$$

and

$$r_\lambda = 4.56\pi \frac{r}{\lambda}, \quad (9)$$

$$\lambda = 5r_m, \quad (10)$$

where  $r$  is the transverse distance measured from the jet axis,  $\phi$  is the azimuthal angle (or phase angle) in the coordinate plane  $(y, z)$ ,  $r_m$  is the radius of the jet, and  $J_0(r_\lambda)$  and  $J_1(r_\lambda)$  are the zeroth and first order Bessel functions. Because the magnetic field is periodic along the jet, we only need to consider a distance of one wavelength,  $\lambda$ , of the periodic spatial field. The components of the field can also be described using the spherical coordinates  $(H, \psi, \eta)$ , as for the homogeneous helical field (Equations (1)–(3)): in this case  $(H, \eta)$  are functions of  $r$ ,  $\phi$  and  $x/\lambda$ . We will assume that the shock is thin and the magnetic field within the shock can be described by the expressions given above for a given  $x$ .

## 2.2 Magnetic Field of the Postshock

Now we derive the expressions for the field components of the postshock. We consider a cylindrical shock propagating along the jet. The speed of the jet flow is  $c\beta_j$  (Lorentz factor  $\gamma_j$ ). The magnetic field is assumed to be frozen into the jet plasma and is described by the expressions of  $(H_x, H_y, H_z)$  given in the last section. The speed of the shock is denoted by  $c\beta_s$  (Lorentz factor  $\gamma_s$ ). Thus, the velocity of the shock relative to the jet plasma,  $c\beta_{sj}$ , and the corresponding Lorentz factor  $\gamma_{sj}$  are given by the following equations,

$$\beta_{sj} = \frac{\beta_s - \beta_j}{1 - \beta_s \beta_j}, \quad (11)$$

and

$$\gamma_{sj} = \gamma_s \gamma_j (1 - \beta_s \beta_j) \approx \frac{\gamma_s}{2\gamma_j}. \quad (12)$$

For an extremely relativistic shock, ( $\gamma_{sj} > 1$ ),  $\gamma_{sj} \approx \frac{\gamma_s}{2\gamma_j}$ , and the Lorentz factor of the postshock plasma  $\gamma_{ps} \approx \gamma_s/\sqrt{2}$  (Blandford & McKee 1976; Königl 1980). The transverse field component of the postshock is amplified by shock compression and the amplification factor is  $\sim 2\sqrt{2}\gamma_{sj} \approx \sqrt{2}\gamma_s/\gamma_j$ . The longitudinal field component remains unchanged. Therefore the magnetic field in the postshock region (in the comoving frame) can be expressed as:

$$H_{ps,x} = H_x, \quad (13)$$

$$H_{ps,y} = \frac{\sqrt{2}\gamma_s}{\gamma_j} H_y, \quad (14)$$

$$H_{ps,z} = \frac{\sqrt{2}\gamma_s}{\gamma_j} H_z. \quad (15)$$

In the observer's frame the magnetic field components of the postshock are:

$$H_{obs,x} = H_{ps,x}, \quad (16)$$

$$H_{obs,y} = \gamma_{ps} H_{ps,y}, \quad (17)$$

$$H_{obs,z} = \gamma_{ps} H_{ps,z}. \quad (18)$$

### 2.3 Polarization Position Angle

As shown by Björnson (1982) (also see Blandford & Königl 1979; Königl & Choudhuri 1985b), for a relativistically moving synchrotron source with its magnetic field configuration in its comoving frame as shown in Figure 1, the observed polarization position angle  $\xi$  can be written as:

$$\tan \xi = \cot \eta_{ps} (-\cos \theta_* + \cot \psi_{ps} \sec \eta_{ps} \sin \theta_*). \quad (19)$$

Here  $\eta_{ps}$  and  $\psi_{ps}$  are the polar and azimuthal angles of the magnetic field in the postshock frame,  $\theta_*$  is the aberration angle, satisfying

$$\cos \theta_* = \frac{\cos \theta - \beta_{ps}}{1 - \beta_{ps} \cos \theta}, \quad (20)$$

and

$$\sin \theta_* = \frac{\sin \theta}{\gamma_{ps}(1 - \beta_{ps} \cos \theta)}, \quad (21)$$

where  $\gamma_{ps} = (1 - \beta_{ps}^2)^{-\frac{1}{2}}$ . If we write the polarization angle in terms of the magnetic field components in the observer's frame, then

$$\tan \xi = \frac{\cot \eta_{obs}}{(1 - \beta_{ps} \cos \theta)} (-\cos \theta + \beta_{ps} + \cot \psi_{obs} \sec \eta_{obs} \sin \theta). \quad (22)$$

Here we note that the relativistic transformation for the magnetic field from the postshock frame to the observer's frame is:  $\tan \psi_{obs} = \gamma_{ps} \tan \psi_{ps}$ ,  $\eta_{obs} = \eta_{ps}$  ( $\xi$  is again an invariant).

We can also use the magnetic field components to write down these formulae: in the postshock frame,

$$\tan \xi = \frac{H_{ps,y}}{H_{ps,z}} \left( -\cos \theta_* + \sin \theta_* \frac{H_{ps,x}}{H_{ps,y}} \right), \quad (23)$$

or in terms of the field components in the observer's frame,

$$\tan \xi = \frac{H_{obs,y}/H_{obs,z}}{1 - \beta_{ps} \cos \theta} \left( \beta_{ps} - \cos \theta + \sin \theta \frac{H_{obs,x}}{H_{obs,y}} \right). \quad (24)$$

Here we note that the relativistic transformation gives:  $H_{\text{obs},x} = H_{\text{ps},x}$ ,  $H_{\text{obs},y} = \gamma_{\text{ps}} H_{\text{ps},y}$ ,  $H_{\text{obs},z} = \gamma_{\text{ps}} H_{\text{ps},z}$ . The polarization angle swing occurs when  $\beta_{\text{ps}} \sim \cos\theta$  and the transverse field component rotates through the position where  $H_y/H_z \gg 1$  (Königl & Choudhuri 1985b; Blandford & Königl 1979).

## 2.4 Stokes Parameters

In order to study the polarization properties of a relativistically moving synchrotron source (shock) we need to use the Stokes parameters to describe the radio emission of the postshock. We will first calculate the Stokes parameters in the comoving frame and then transform them to the observer's frame through a Lorentz transformation (Björnson 1982; Königl & Choudhuri 1985b; Qian 1992). The Lorentz transformation involved is quite simple. What we need to do is just to multiple each of the Stokes parameters by a factor  $D_{\text{ps}}^{3+\alpha}$  (Björnson 1982; Qian 1992). Here  $D_{\text{ps}} = [\gamma_{\text{ps}}(1 - \beta_{\text{ps}}\cos\theta)]^{-1}$  is the Doppler factor of the postshock emitting plasma,  $\alpha$  is the spectral index (defined as  $S_\nu \propto \nu^{-\alpha}$ ). For simplicity we only consider optically thin radio frequencies. We assume that the shock is thin in the sense that the magnetic field in the postshock region is uniform, although the field changes along the jet. We also assume that the energy distribution of the relativistic electrons is isotropic, having a power-law form of an index of  $2\alpha + 1$  (i.e.,  $N_{\text{ps}} \propto E^{-(2\alpha+1)}$ ), but the number density of relativistic electrons may have a distribution across the cross-section of the jet (see below). For an unresolved postshock emitting region the Stokes parameters ( $I_0, Q_0, U_0$ ) of the synchrotron radiation can be obtained by integration over the whole cross-section. Then we have:

$$I_0 = D_{\text{ps}}^{3+\alpha} \int I_\sigma d\sigma, \quad (25)$$

$$Q_0 = D_{\text{ps}}^{3+\alpha} \frac{3+3\alpha}{5+3\alpha} \int I_\sigma \cos 2\xi d\sigma, \quad (26)$$

$$U_0 = D_{\text{ps}}^{3+\alpha} \frac{3+3\alpha}{5+3\alpha} \int I_\sigma \sin 2\xi d\sigma. \quad (27)$$

The corresponding expression for the polarized flux density is

$$P_0 = (Q_0^2 + U_0^2)^{\frac{1}{2}}, \quad (28)$$

where

$$I_\sigma(r) = (1+z')^{1-\alpha} C_5 (2C_1)^\alpha \nu^{-\alpha} N_{\text{ps},0} \times \exp[-(r/r_m)^2] (H_{\text{ps}} \sin \mu_{\text{ps}})^{1+\alpha} D_l^{-2} \Delta x, \quad (29)$$

$$\sin^2 \mu_{\text{ps}} = \cos^2 \psi_{\text{ps}} [\tan^2 \psi_{\text{ps}} (1 - \sin^2 \theta_* \cos^2 \eta_{\text{ps}}) + \sin^2 \theta_* - \sin 2\theta_* \cos \eta_{\text{ps}} \tan \psi_{\text{ps}}]. \quad (30)$$

Here  $z'$  is the redshift,  $I_\sigma$  is the intensity of synchrotron radiation emitted by a small element of the cross-section of the postshock ( $d\sigma$ ),  $\theta_*$  is the aberration angle,  $\Delta x$  is the thickness of the postshock.  $\int d\sigma$  represents the integration over the entire cross-section of the postshock,  $\nu$  is the observing frequency,  $\xi$  is the polarization position angle of the emitting element of the postshock as given above,  $C_5 \equiv C_5(\alpha)$  and  $C_1$  are constants (see Pacholczyk 1970).  $N_{\text{ps},0}$  is the normalization of the relativistic electron energy distribution, being a function of  $r$  in the form of  $\exp[-(r/r_m)^2]$  ( $r_m$  is the radius of the jet),  $H_{\text{ps}}$  is the strength of magnetic field of the postshock,  $\mu_{\text{ps}}$  is the angle between the magnetic field and the direction to the observer. We should point out that when this angle is calculated (or it is transformed from the observer's frame to the postshock frame), we should use a relativistic transformation for an angle between

two directions neither of which coincides with the direction of motion (see Pacholczyk 1970). The transformation insures the angle between the two directions projected on the plane perpendicular to the direction of motion to be Lorentz invariant. So the angle  $\psi_{\text{ps}}$  in the equation (30) for  $\mu_{\text{ps}}$  is given by

$$\cos\psi_{\text{ps}} = \frac{\cos\psi_{\text{obs}} - \beta_{\text{ps}}}{1 - \beta_{\text{ps}}\cos\psi_{\text{obs}}}, \quad (31)$$

where  $\psi_{\text{obs}}$  is related to the polar angle of the magnetic field  $\mathbf{H}_{\text{obs}}$  in the observer's frame.

We point out that in the previous studies of large polarization angle swings (e.g. Blandford & Königl 1979; Björnson 1982; Königl & Choudhuri 1985b) results are given only for the angle and degree of polarization. Although these two parameters are important for describing the properties of the source polarization, they are independent of the Doppler factor and cannot give information on the relationship between the polarization angle swing and the variations in flux density and polarized flux density. Therefore, in this paper we will give results for the three parameters: angle of polarization ( $\xi$ ), flux density ( $I_0$ ) and polarized flux density ( $P_0$ ).

### 3 POLARIZATION ANGLE SWING CAUSED BY ROTATION OF MAGNETIC FIELD

Specific models have been made to show the results for polarization angle swings, using the given configurations of magnetic field. The following parameters are used:  $\gamma_j = 1.5$ ,  $\gamma_s = 9.0$ ,  $\beta_{\text{ps}} = 0.98758$  ( $\gamma_{\text{ps}} = 6.36$ ),  $\theta = 8^\circ$ ,  $\alpha = 1.0$ ,  $r_m = 0.2\lambda$ . It is not necessary to specify the other parameters (e.g.  $N_{\text{ps},0}$ ,  $H_{\text{ps}}$ ,  $\lambda$ ,  $\Delta x$ ,  $\nu$ , etc.) because we use relative units in the computation of  $I_\sigma$ . We choose  $\theta(\text{radian}) \sim 1/\gamma_{\text{ps}}$ . In this case the polarization position angle swing is fast and the Doppler beaming is strong, hence it will be easily observed. In the following figures the flux density ( $I_0$ ) and polarized flux density ( $P_0$ ) and polarization angle ( $\xi$ ) are calculated by using the formulae (23) and (25)–(30).

#### 3.1 Homogeneous Helical Field

We choose  $\eta = 70^\circ$  to specify the helical field. In Figure 2 are shown the results for the homogeneous helical field: the light curves of the total flux, polarized flux density and polarization angle swing. It can be seen that rapid swing occurs at  $x/\lambda \sim 0.65$ – $0.85$ , and the greatest rate of swing is at  $x/\lambda = 0.75$ . The most prominent property of the swing is that during the period of swing of  $\sim 180^\circ$  the flux density and the polarized flux density vary only very little (in the interval of  $x/\lambda$  from 0.65 to 0.85, only vary by  $\sim 3\%$ ). The polarization degree remains constant.

#### 3.2 Force-free Magnetic Field

The results for the force-free field configuration are shown in Figure 3. It can be seen that rapid swing of  $\sim 180^\circ$  occurs at  $x/\lambda \sim 0.4$ – $0.6$ , the most rapid is at  $x/\lambda = 0.5$ . The most prominent property of the swing is that during the swing period, the polarized flux density has a minimum coinciding with the maximal rate of polarization angle swing, while the flux density is almost constant. This indicates that the polarization degree varies rapidly during the swing and has a minimum (decreasing from  $\sim 65\%$  to  $\sim 35\%$ ) at the maximal swing.

Here we see that for the force-free field (mode  $m=1$ ) the variability of polarized flux density is completely different from that for the homogeneous helical field. These different properties may be useful for distinguishing the different models.

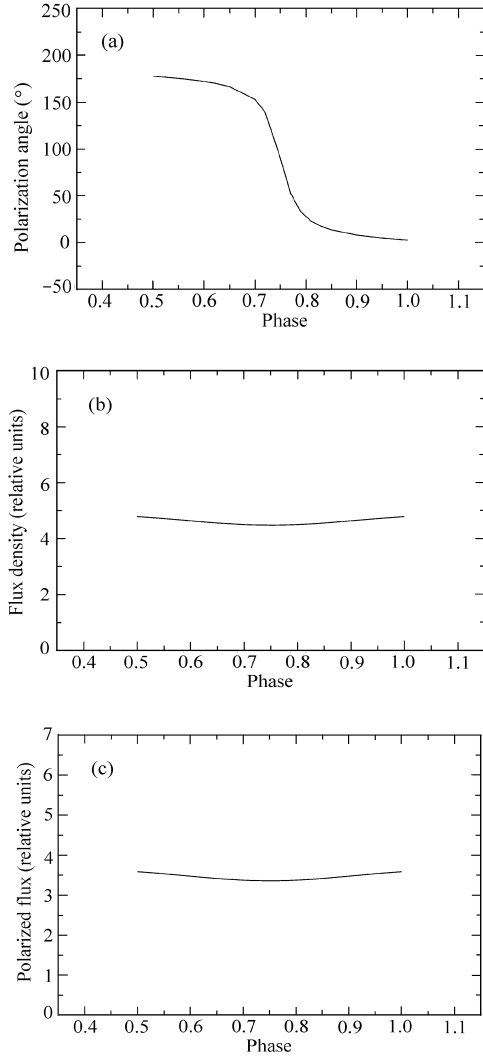


Fig. 2 The case of a relativistic shock propagating through a homogeneous helical field. (a) Polarization position angle swing, (b) the flux density light curve. (c) the polarized flux density light curve.

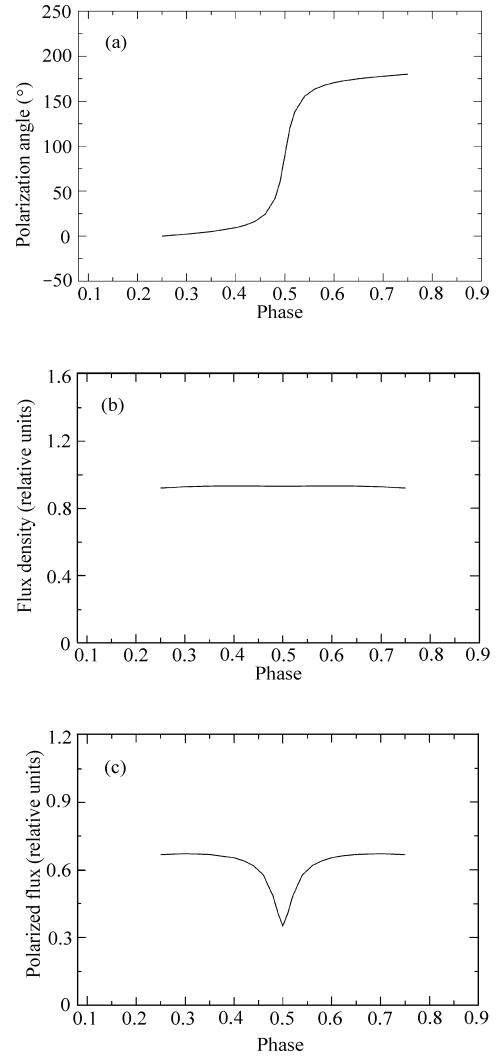


Fig. 3 The case of a relativistic shock propagating through a force-free magnetic field. (a) Polarization angle swing, (b) the flux density light curve, and (c) the polarized flux density light curve.

#### 4 POLARIZATION ANGLE SWING CAUSED BY CHANGE OF VIEWING ANGLE

We have also calculated the behavior of polarization angle swing and variability of flux density and polarized flux density for the case in which the viewing angle (or the aberration angle) changes due to variation in the dynamical behavior of the shock. For the chosen parameters

( $\beta_{\text{ps}}=0.98758$  and  $\gamma_{\text{ps}}=6.36$ ) the relation between the viewing angle and the aberration angle is shown in Figure 4.

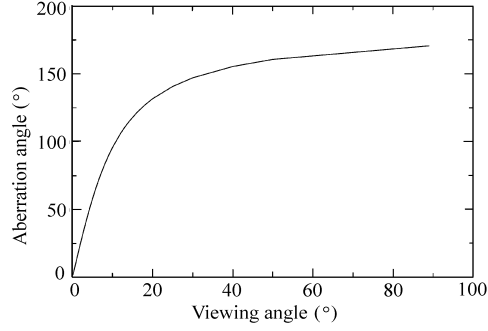


Fig. 4 Relation between the aberration angle  $\theta_*$  and the viewing angle  $\theta$ .

#### 4.1 Homogeneous Helical Field

We consider a fixed field orientation and let the viewing angle vary. Because the amplitude of polarization angle swing is much smaller than  $180^\circ$  for  $x/\lambda \gg 0.75$ , the results are given for a fixed value of  $x=0.72$  and shown in Figure 5. It can be seen that the polarization angle swing

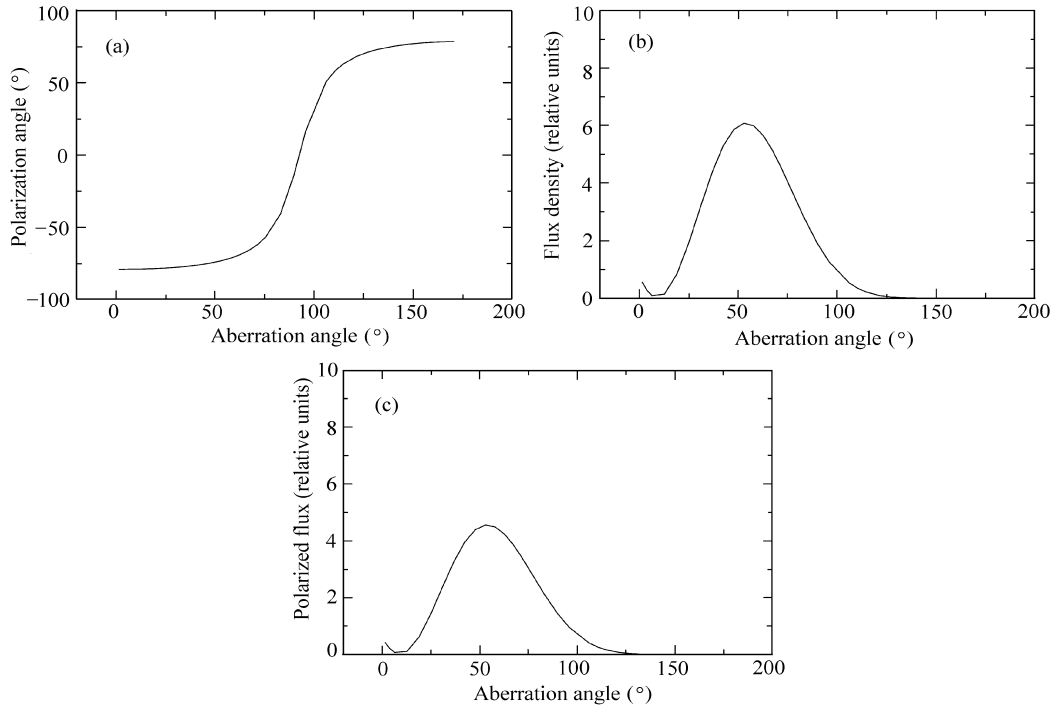


Fig. 5 (a) Polarization angle swing caused by changes of viewing angle for the case of homogeneous magnetic field; (b) and (c), light curves of the flux density and of the polarized flux density.

is  $\sim 150^\circ$ , and that the swing occurs when the aberration angle varies from  $\sim 60^\circ$  to  $\sim 120^\circ$ . The greatest rate of swing is at  $\theta_* \sim 90^\circ$  (corresponding  $\cos\theta \sim \beta_{\text{ps}}$ ). We found that both the flux density and polarized flux density decrease during the time of swing while the degree of polarization remains constant. This property is mainly due to the changing Doppler boosting.

## 4.2 Force-free Magnetic Field

We also consider a fixed field structure of the postshock region. Because the amplitude of polarization angle swing is much smaller than  $180^\circ$  for  $x/\lambda \gg 0.50$ , so we give only the results for a fixed value of  $x/\lambda=0.48$  (Figure 6). It can be seen that the properties of the swing are similar to that for the homogeneous field. The greatest rate of swing occurs also at  $\theta_* \sim 90^\circ$ . The swing is  $\sim 150^\circ$  and during the swing the flux density and polarized flux density decrease due to the changes in the Doppler boosting, but the polarization degree remains constant.

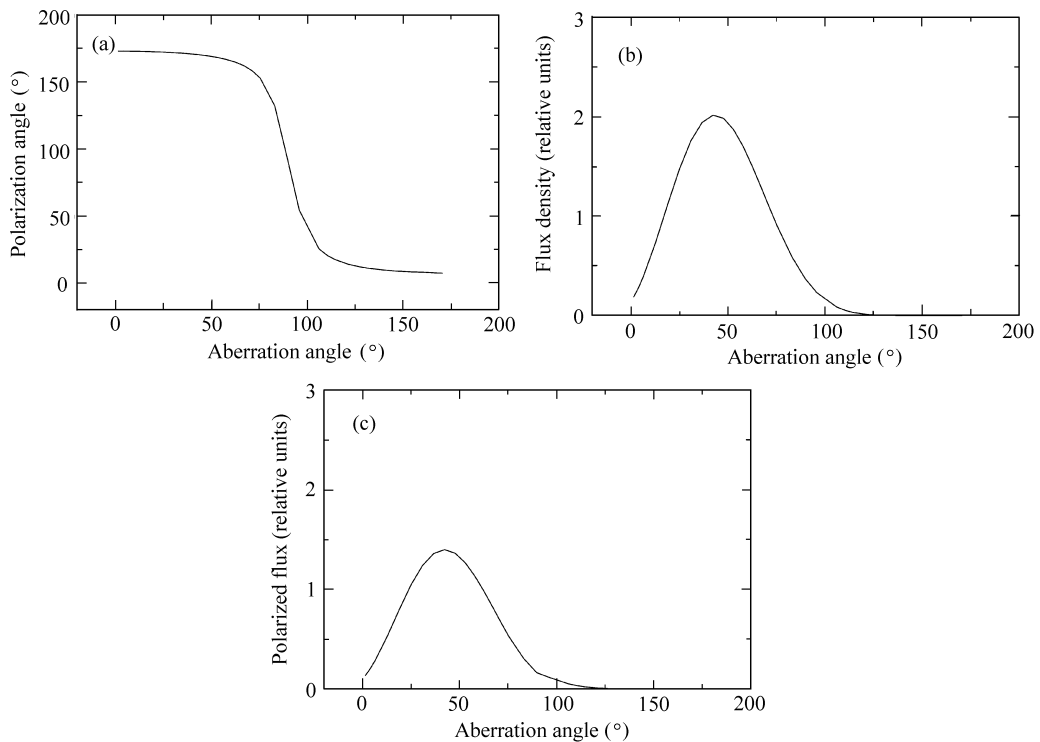


Fig. 6 (a) Polarization angle swing caused by the change of viewing angle for the case of a force-free magnetic field; (b) and (c), light curves of the flux density and of the polarized flux density.

## 5 DISCUSSION

1. It can be seen from Figures 2–3 and 5–6 that polarization angle swings of  $\sim 180^\circ$  can occur for both configurations (force-free field (mode  $m=1$ ) and homogeneous helical field), but the pattern of variability of polarized flux density and flux density is different in the two configurations. In the case of polarization angle swing due to the rotation of transverse

field component, the properties are significantly different for the homogeneous helical field and the force-free field: (1) For the force-free (mode  $m=1$ ) configuration, the interesting feature is that the polarized flux density (or polarization degree) reaches a minimum when the polarization angle swing is most rapid; (2) For the homogeneous helical field configuration, during the polarization angle swing the polarized flux density (and also polarization degree) remains almost constant.

2. In the case of polarization angle swing due to change of viewing angle, the properties of the swing are quite similar for both the homogeneous field and the force-free field. The polarization angle swing occurs at  $\theta_* \sim 90^\circ$  (corresponding  $\cos\theta \sim \beta_{ps}$ ) and during the swing the flux density and the polarized flux density decrease by a large factor. For the value chosen for  $\gamma_{ps}$  the swing occurs when the viewing angle changes from  $\sim 6^\circ$  to  $\sim 18^\circ$  (corresponding to  $\theta_*$  changing from  $\sim 60^\circ$  to  $\sim 120^\circ$ ).

Finally we should point out that all the models of polarization angle swing discussed in this paper are single-component models, i.e., the shock component is the only polarized emission region. If another polarized component with comparable polarization (steady or variable) exists, then the resultant polarized emission will be a vector combination of these two polarized components. In this case rapid polarization angle swing of  $\sim 180^\circ$  may not be observed, but the polarization angle swing of the shock component will cause a rapid variation of the integrated polarization. This could be useful for explaining rapid polarization variability, especially for the cases where rapid polarization variations are not accompanied by substantial intensity variations. In addition, if the magnetic field is not so regular as that we studied in Section 3 the flux density could also vary by a considerable amount during a polarization angle swing. VLBI polarization observations may be useful to find the variable components causing polarization angle swings and so distinguish the different models (intrinsic and extrinsic).

**Acknowledgements** This work was started when S. J. Qian visited the Max-Planck Institut für Radioastronomie. The support from the Institut during his visit is acknowledged.

## References

- Aller H. D., Aller M. F., Hughes P. A., 2002, In: E. Ros, R. W. Porcas, A. P. Lobanov, J. A. Zensus (MPIfR), eds., Proceedings of the 6th European VLBI Network Symposium on New Developments in VLBI Science and Technology, p.111
- Aller M. F., 1999, In: L. O. Takalo, A. Sillanpää, eds., ASP Conference series 159, BL Lac Phenomenon, p.31
- Björnson C.-I., 1982, ApJ, 260, 855
- Blandford R., Königl A., 1979, ApJ, 232, 34
- Blandford R., McKee C. F., 1976, Physics of Fluids, 19, 1130
- Gabuzda D. C., Cawthorne T. V., 2000, MNRAS, 319, 1056
- Gopal-Krishna, Wiita P. J., 1992, A&A, 259, 109
- Hughes P. A., Aller H. D., Aller M. F., 1989, ApJ, 341, 68
- Königl A., 1980, Physics of Fluids, 23, 1083
- Königl A., Choudhuri A. R., 1985a, ApJ, 289, 173
- Königl A., Choudhuri A. R., 1985b, ApJ, 289, 188
- Kochenov P. Yu., Gabuzda D. C., 1999, In: L. O. Takalo, A. Sillanpää, eds., ASP Conference series 159, BL Lac Phenomenon, p.460

- Ledden J. E., Aller H. D., 1978, In: A. M. Wolfe (Pittsburgh University), ed., Pittsburgh Conference on BL Lac objects, p.60
- Marscher A. P., Gear W. K., Treves T. P., 1992, In: E. Valtaoja, M. Valtonen, eds., Variability of Blazars, Cambridge, p.85
- Marscher A. P., 1996, In: J. G. Kirk, M. Camenzind, C. von Montigny, S. Wagner, eds., Proceedings of the Heidelberg Workshop on Gamma-ray Emitting AGN, MPIfK: Heidelberg, p.103
- Pacholczyk A. G., 1970, Radio Astrophysics, San Francisco: Freeman
- Qian S. J., Quirrenbach A., Witzel A., Krichbaum T. P., Hummel C. A., Zensus J. A., 1991, A&A, 241, 15
- Qian S. J., 1992, Chin. A&A, 16, 266
- Qian S. J., 1993, Chin. A&A, 17, 229
- Qian S. J., Witzel A., Kraus A., Krichbaum T. P., Zensus J. A., 2001, A&A, 367, 770
- Qian S. J., Kraus A., Zhang X. Z., Krichbaum T. P., Witzel A., Zensus J. A., 2002, Chin. J. Astron. Astrophys., 2(4), 325
- Quirrenbach A., Witzel A., Qian S. J., Krichbaum T. P., Hummel C. A., Alberti A., 1989, A&A, 226, L1
- Rickett B. J., Quirrenbach A., Wegner R., Krichbaum T. P., Witzel A., 1995, A&A, 293, 479
- Rickett B. J., Kedziora-Chudzcer L., Jauncey D. L., 2002, Proc. Astron. Soc. Aust., 19, 106
- Simonetti H. J., 1991, A&A, 250, L1
- Wagner S., Witzel A., 1995, ARA&A, 33, 163